Analyst

PAPER

View Article Online
View Journal | View Issue



Cite this: *Analyst*, 2015, **140**, 4089

# Surface state of the dopamine RNA aptamer affects specific recognition and binding of dopamine by the aptamer-modified electrodes

Isabel Álvarez-Martos,[a,b] Rui Campos[a,b] and Elena E. Ferapontova*[a,b]

Received 10th March 2015,
Accepted 8th April 2015

DOI: 10.1039/c5an00480b

www.rsc.org/analyst

Specific monitoring of dopamine, in the presence of structurally related neurotransmitters, is critical for diagnosis, treatment and mechanistic understanding of a variety of human neuropathologies, but nevertheless the proper tools are scarce. Recently, an electrochemical aptasensor for specific analysis of dopamine, exploiting dopamine biorecognition by the RNA aptamer electrostatically adsorbed onto a cysteamine-modified electrode, has been reported (*Analytical Chemistry* **85** (2013) 121). However it was not clear which way dopamine biorecognition and binding by such aptamer layers proceed and if they can be improved. Here, we show that the aptamer surface state, in particular the aptamer surface density, in a bell-shaped manner affects the dopamine binding, being maximal for the 3.5 ± 0.3 pmol $cm^{-2}$ monolayer coverage of the aptamer molecules lying flat on the surface. Therewith, the aptamer affinity for dopamine increases one order of magnitude due to electrostatically regulated immobilization, with the aptamer–dopamine dissociation constant of 0.12 ± 0.01 μM *versus* 1.6 ± 0.17 μM shown in solution. Under optimal conditions, 0.1–2 μM dopamine was specifically and 85.4 nA $\mu M^{-1}$ $cm^{-2}$ sensitively detected, with no interference from structurally related catecholamines. The results allow improvement of the robustness of dopamine monitoring by aptamer-modified electrodes in biological systems, within the 0.01–1 μM dopamine fluctuation range.



## Introduction

Dopamine is an important neurotransmitter (NT) in the central nervous system that regulates movement, endocrine function, reward behavior, and memory processes.[1] A variety of human pathologies have been linked to alterations in neuronal release and uptake of dopamine, such as neuropsychiatric disorders (depression, schizophrenia, attention deficit hyperactivity disorder),[2] neurodegenerative diseases (Parkinson's disease),[3] and drug addiction.[4,5] As a result of its biological and medical significance, precise and selective *in vivo* analysis of dopamine at its 10 nM–1 μM levels characteristic of living systems[6] is of great significance for clinical diagnosis and monitoring of treatment of the diseases and understanding mechanisms of their development.

Traditionally, detection of dopamine is performed *via* well-established "separation and detection" techniques.[7] Although these methods provide high sensitivity of dopamine analysis, they have such drawbacks as (i) the requirement of sample pre-treatment, (ii) poor spatial resolution, (iii) complexity of the accompanying technical set-up, and (iv) long analysis times. With the aim of understanding the NT metabolism and their function *in vivo*, many efforts have been focused on developing invasive electrochemical sensors,[8] which allow real-time detection and millisecond-range responses, can be easily miniaturized and are cost-effective. However, the selectivity of the electrochemical sensors for dopamine analysis may be compromised by the presence of other chemically-related neurotransmitting molecules with similar redox potentials such as catechol, norepinephrine, epinephrine, levodopa (L-DOPA) and some other,[9] and interference from other species with overlapping oxidation potentials such as ascorbic acid (AA) and uric acid (UA).[10,11] To overcome AA and UA interference the surface of the electrodes can be either electrochemically pre-treated[12] or chemically modified with a wide range of materials, including self-assembled monolayers, metal nanoparticles and metal oxides, conducting polymers, graphene and its composites with nanoparticles, carbon nanotubes, nanowires, and permselective membranes,[13] these modifications demonstrating improved selectivity and sensitivity of analysis in the presence of AA and UA.[8] Despite all innovative technologies, the major problem of interference of other structurally related NTs with the selective analysis of dopamine has not been overcome.

[a]*Interdisciplinary Nanoscience Center (iNANO), Aarhus University, Gustav Wieds Vej 1590-14, DK-8000 Aarhus C, Denmark. E-mail: elena.ferapontova@inano.au.dk*
[b]*Danish National Research Foundation: Center for DNA Nanotechnology (CDNA), Aarhus University, Gustav Wieds Vej 1590-14, DK-8000 Aarhus C, Denmark*

Recently, we have reported an electrochemical RNA-aptamer based biosensor for specific analysis of dopamine in the presence of other NTs.[9] High specificity of ligand binding by aptamers makes them excellent antibody-competitive biorecognition units for selective and sensitive analysis of a variety of analytes,[14,15] including such small molecules of clinical interest as cocaine and theophylline.[16,17] In the particular case of dopamine, the aptamer-based biosensor allowed the clinically required sensitivity and selectivity of dopamine analysis in the presence of structurally related NTs that were electrochemically active in the same potential window as dopamine itself.[9] The aptamer was immobilized onto the positively charged cysteamine-modified electrode surface (Fig. 1) and demonstrated a 0.1 μM dopamine detection limit and a physiologically relevant linear range of 100 nM–5 μM, where no interference from such structurally related NTs such as norepinephrine, epinephrine, L-DOPA, DOPAC, catechol, tyramine, and methyldopamine was observed.

Although it was not completely understood how the aptamer immobilization at the electrode surface affected the aptamer–ligand biorecognition, we found a strong inconsistency between the aptamer and aptamer-bound dopamine surface coverages[9] (discussed in more detail later). It was clear that the surface state and concentration of the aptamer should be critical for sensitive and selective binding of dopamine. Both factors are known to dramatically affect DNA–DNA interactions[18] and electron transfer (ET) reactions between electrode-tethered DNA and redox indicators either covalently attached to DNA or present in solution,[19,20] and thus are to be implicated in dopamine–aptamer binding. In this context, electrochemical activity of dopamine as a ligand offered a unique opportunity to correlate binding properties of the aptamer (followed *via* dopamine electrochemistry) with the surface state of the aptamer (analysed from electrochemical responses of a redox label conjugated to the aptamer sequence, Fig. 1).

Here, we studied the effect of the aptamer surface population and state on the dopamine binding ability, in order to correlate the activity of the aptamer, in the reaction of dopamine biorecognition and binding, with its surface state. We kept in mind that aptasensor properties are apparently predetermined not by the overall number of the aptamer probe molecules at the electrode surface, but only by those that are able to capture the target analyte, dopamine. The probe surface density leading to the overcrowded interfacial environment may impede specific binding of dopamine by restricting the aptamer accessibility for dopamine molecules and capability of conformational changes concomitant with the dopamine binding. The specific dopamine-binding ability of the aptamer that preconditions the overall sensor performance has been assessed by correlating signals from the methylene blue (MB)-labeled dopamine-specific RNA aptamer with those from the aptamer-bound dopamine, in order to establish conditions ensuring reliable analysis of the analyte.

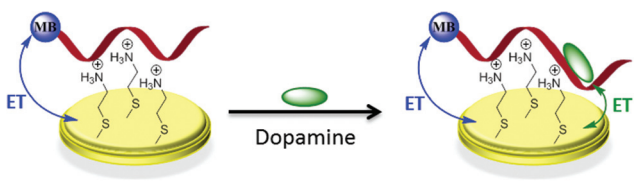


Fig. 1 Schematic representation of the Methylene Blue (MB)-labeled aptamer immobilization and dopamine binding at the aptamer-modified electrode surface.

## Experimental section

### Materials and reagents

Dopamine, norepinephrine, catechol, L-DOPA, ethanol (96%), $Na_2HPO_4$, $NaH_2PO_4$, NaCl, and cysteamine were purchased from Sigma-Aldrich (Germany). All chemicals were of analytical grade and used as received. The 57-mer Dopa_RNA aptamer for dopamine (5′-GUC UCU GUG UGC GCC AGA GAC AGU GGG GCA GAU AUG GGC CAG CAC AGA AUG AGG CCC-3′)[21] was synthesized by RiboTask (Denmark). The 5′-MB-labeled aptamer was prepared as previously described[9] from 5′-amino-$C_6$-modified RNA aptamer obtained from RiboTask (Denmark). Water was purified by a Milli-Q reference A+ water purification system (18 MΩ, Millipore, Bedford, MA, USA). Stock solutions of catecholamines were prepared daily in 20 mM phosphate buffer solution containing 0.15 M NaCl (PBS), pH 7.4, and protected from light until analysis.

### Instrumentation

Cyclic voltammetry (CV) and chronoamperometry (CA) measurements were performed in a conventional three-electrode electrochemical cell consisting of a gold working electrode (0.2 cm in diameter, CH Instruments, Austin, TX), an Ag/AgCl (3 M KCl) as the reference electrode (Metrohm, Denmark), and a platinum wire counter electrode, with a potentiostat AUTOLAB PGSTAT 30 (Eco Chemie B.V., Utrecht, The Netherlands) equipped with a NOVA 1.10 software. Working solutions were degassed with $N_2$ for at least 5 min prior data acquisition and kept under $N_2$ during the entire experiment. The reproducibility of the data was verified by measurements with at least four equivalently prepared electrodes. All measurements were performed at 22 ± 1 °C.

### Electrode modification

Prior modification, gold disk electrodes were cleaned in 0.5 M NaOH by potential cycling at 0.05 V $s^{-1}$, hand-polished to a mirror luster in 1 μm diamond and 0.1 μm alumina slurries (Struers, Denmark) on microcloth pads (Buehler, Germany), and ultrasonicated in ethanol/water solutions for 15 min. Afterwards, they were electrochemically polished in 1 M $H_2SO_4$ and 0.5 M $H_2SO_4$/10 mM KCl at 0.3 V $s^{-1}$. The electrode surface area was determined by integrating the reduction peak of gold surface oxide during the final scan in 0.1 M $H_2SO_4$, assuming a theoretical value of 400 μC $cm^{-2}$ for a monolayer of chemisorbed oxygen on gold electrode,[22] and was typically 0.084 ± 0.005 $cm^2$. The electrodes were further water-rinsed

 

and kept in ethanol for 30 min before modification. The electrodes were modified with cysteamine by placing a 10 μL drop of a 20 mM cysteamine solution onto the electrode surface (for 2 h under the lid). After a thorough rinse in PBS, the surface of the cysteamine-modified electrodes was exposed to 10 μL of a 10 μM aptamer solution. The aptasensor was stored at 4 °C between measurements. All solutions containing MB-aptamer/MB-aptamer modified electrodes were kept in the dark.

## Results and discussion

The surface coverage of the dopamine-specific RNA aptamer electrostatically adsorbed onto the cysteamine SAM-modified gold electrode, determined in our previous work by integration of the MB redox peaks in cyclic voltammograms (CVs) recorded with a MB-conjugated RNA aptamer, was 6.6 ± 0.5 pmol $cm^{-2}$ (referred to the electrochemically active surface area).[9] This surface coverage corresponds to a densely packed aptamer surface state, approaching the theoretical limiting surface coverage of vertically standing DNA duplexes of around 5.2 × $10^{12}$ molecules $cm^{-2}$ (equivalent to 8.3 pmol $cm^{-2}$).[23] Obviously, the aptamer surface coverage of 6.6 pmol $cm^{-2}$ is inconsistent with a monolayer of electrostatically adsorbed (and thus lying flat) ligand-active aptamer species. Along with that, electroanalysis of dopamine binding to the unlabeled RNA aptamer immobilized at the electrode gave 1.86 ± 0.12 pmol $cm^{-2}$ of bound dopamine (equivalent to the active aptamer surface coverage), and it is evident that such discrepancy can be due to the restricted dopamine binding ability of the aptamer in a densely populated aptamer monolayer or even a multilayer assembly. Adsorption of random coiled DNA on positively charged surfaces has also been reported to be accompanied by tangling and overlaying of DNA molecules in a multilayer film with a restricted ability for hybridization.[24,25]

Thus, the MB-labeled RNA aptamer was immobilized onto the positively charged cysteamine self-assembled monolayer (SAM)-modified gold electrode, and its dopamine-binding ability was studied as a function of the aptamer surface coverage, $\Gamma_{RNA}$, calculated by integrating the voltammetric signals stemming from either the MB redox transformation at −260 mV (the absolute aptamer surface coverage) or oxidation of the aptamer-bound dopamine at 200 mV (the dopamine-active aptamer surface coverage) (Fig. 2). Both surface coverages were calculated according to the equation: $\Gamma_{RNA} = Q/nFA$, where $Q$ is the charge associated with the redox peaks of either MB or dopamine, $n$ is the number of electrons involved in the redox process, $n = 2$ for both reactions, $F$ is Faraday's constant, and $A$ is the electroactive surface area. The varying surface coverage of the aptamer was controlled by varying the aptamer immobilization time.

CV analysis of dopamine signals at the aptamer-modified electrodes demonstrated immediately a very different apparent sensitivity of analysis followed for different immobilization times, with the CV peak current intensities of dopamine oxidation being essentially lower in the case of longer aptamer

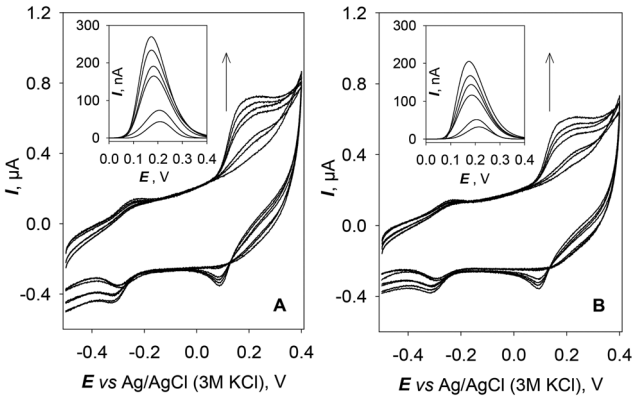


**Fig. 2** Representative CVs recorded with the aptamer-modified electrodes prepared by (A) 0.5 h and (B) 2 h aptamer immobilization, in PBS, pH 7.4, containing of 1, 2, 4, 6, 8 and 10 μM dopamine. Inset: background-corrected CV peaks of dopamine oxidation. The arrows designate the increasing dopamine concentration. Potential scan rate is 0.1 V $s^{-1}$, a polynomial baseline correction in the insets.

immobilization times (Fig. 2, data for 0.5 h (A) *versus* 2 h (B) immobilization are presented).

Thus, the absolute aptamer surface coverage $\Gamma_{RNA}$ increased with the increasing immobilization time (Fig. 3A) and approached a saturation limit at 7.3 ± 0.3 pmol $cm^{-2}$, for times exceeding 2 h. Along with that, storage of the aptamer-modified electrodes in the buffer solution for 1 h removed the weakly adsorbed species with the desorption rate of 2.99 pmol $cm^{-2}$ $h^{-1}$, the surface coverage being reduced to 3.7 ± 0.4 pmol $cm^{-2}$. After 1 h storage in PBS, the aptamer desorption slowed down to 0.33 pmol $cm^{-2}$ $h^{-1}$, and the $\Gamma_{RNA}$ remained close to the 1 h values (RSD 12%) for at least 3 hours regardless of the time used for the aptamer immobilization (Fig. 3B). For short immobilization times (0.5 h) the absolute aptamer surface coverage reached only 3.5 ± 0.3 pmol $cm^{-2}$ and did not significantly change upon further storage. This variability in the surface adsorption behavior with immobilization time may be ascribed to the weaker adsorption and thus higher desorption rates of the long-time adsorbed aptamer, also due to the formation of the aptamer multilayers. Desorption of the aptamer molecules forming these multilayers from the electrode surface should finally result in the residual aptamer monolayer strongly attached to the positively charged cysteamine SAM.

In general, the anodic peak intensities ($I_{pa}$) stemming from the oxidation of the aptamer-bound dopamine (such as in Fig. 3B, inset) should be proportional to the surface coverage of the dopamine-binding aptamer species according to the equation:[26]

$$I_{pa} = (n^2F^2/4RT)\Gamma_{RNA}A\nu \quad (1)$$

and reach their maximum values at the maximum surface coverage. However, the $\Gamma_{RNA}$ dependence of the dopamine oxidation signals reflecting the dopamine binding ability of the immobilized aptamer had a bell-shaped form, with a maximum at the absolute aptamer surface coverage of 3.5 ±

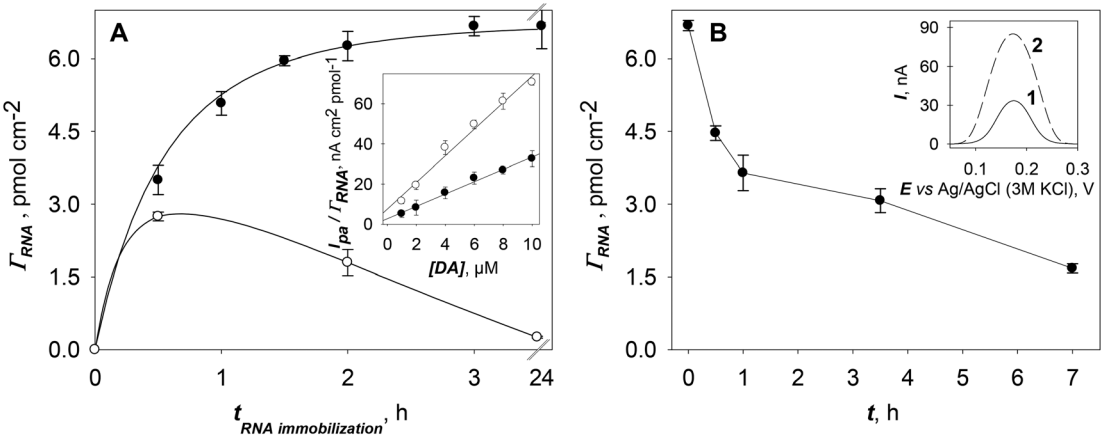


**Fig. 3** (A) Dependence of the aptamer surface coverage ($\Gamma_{RNA}$) on the aptamer immobilization time, $\Gamma_{RNA}$ was estimated by integration of: (black circles) MB redox peaks (a solid line is Sigma Plot fitting to a hyperbolic increase function) and (empty circles) 2 μM dopamine oxidation peaks in CVs recorded with the MB-labeled aptamer/cysteamine-modified gold electrodes. Inset: dopamine concentration dependence of the dopamine oxidation peak currents related to the total amount of the aptamer at the electrode surface for: (black circles) 2 h and (empty circles) 0.5 h of the aptamer immobilization. (B) Variation of the $\Gamma_{RNA}$ (overnight immobilization, MB signals) on time, for the aptamer-modified electrodes stored in PBS between measurements. Inset: background-corrected oxidation peaks of 2 μM dopamine, CVs recorded with the aptamer-modified electrode prepared by the overnight immobilization, (1) freshly prepared electrode and (2) after 1 h incubation in PBS. All data were derived from CVs recorded in PBS, potential scan rate 0.1 V s$^{-1}$. Surface coverage relates to the electrochemically active electrode surface area.

0.3 pmol cm$^{-2}$, and decreased with the increasing absolute $\Gamma_{RNA}$ (Fig. 3A, curve 2). This surface coverage (corresponds to $21 \times 10^{11}$ molecules cm$^{-2}$) is indeed consistent with the RNA aptamer monolayer coverage with a footprint of the RNA aptamer molecule of 47.6 ± 4.1 nm$^2$. If an RNA molecular diameter of 2 nm is assumed, derived as an extreme value from the DNA duplex diameter, then this footprint corresponds to the 0.42 ± 0.04 nm per base stretched RNA molecules adsorbed flat on the electrode surface. For comparison, the B-DNA duplex stretch per base pair may be estimated as 0.34 nm and that of RNA-A as 0.28 nm.[27]

These results evidence that for the aptamer surface coverage exceeding the monolayer, the excessive aptamer adsorption achieved with longer immobilization times did not increase the response of the aptamer-modified electrode towards dopamine (that should result from the enhanced dopamine binding), but *vice versa* (Fig. 3A, inset). This observation is in agreement with the concomitant loss of the aptamer affinity for dopamine molecules as the electrode surface becomes more and more crowded with the aptamer molecules that become more and more restricted in their dopamine-binding ability.

To further understand interactions underlying dopamine and aptamer binding we took into account the surface electrochemistry of dopamine oxidation at its concentrations below 2 μM (a characteristic linear dependence of the oxidation peak currents on the potential scan rate). Under these conditions the dopamine binding to the aptamer followed the Langmuir isotherm behavior (at dopamine concentrations higher than 2 μM there was a strong contribution from dopamine diffusing from the bulk solution to the electrode (Fig. 4)). Keeping in mind a 1 : 1 stoichiometry of the RNA aptamer–dopamine

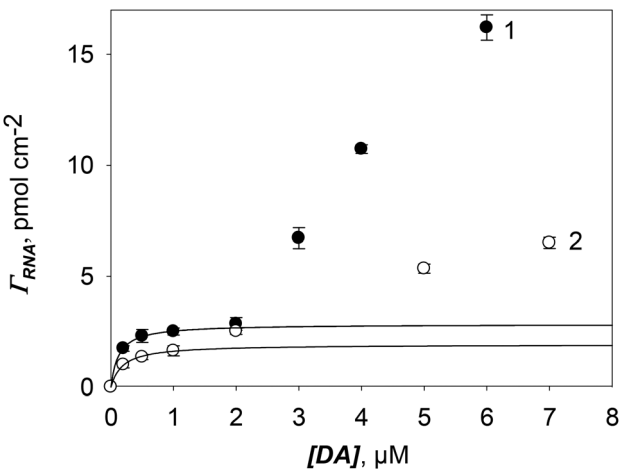


**Fig. 4** The aptamer surface coverage $\Gamma_{RNA}$ estimated by integration of dopamine oxidation peaks recorded with the 0.5 h (1) and 2 h (2) aptamer/cysteamine/Au electrodes in solutions containing different concentrations of dopamine. Data on 2 h immobilization are derived from our previous work[9] and are included for comparison and discussion. The $\Gamma_{RNA}$ relates to the electrochemically active electrode surface area. Solid lines are fitting to the Langmuir adsorption isotherm.

complex, integration of the CV peaks corresponding to the 2e$^-$ oxidation of the aptamer-bound dopamine allowed estimations of the surface population of the dopamine-active aptamer by fitting the data both to the Langmuir adsorption isotherm:[28]

$$\Gamma = (\Gamma_{max} K_b[DA])/(1 + K_b[DA]) \quad (2)$$

 

and the Scatchard model:[29]

$$\Gamma = (\Gamma_{max}[DA])/(K_d + [DA]) \quad (3)$$

where $\Gamma$ is the dopamine surface coverage, $K_b$ reflects the ratio between the dopamine binding and dissociation rate constants at the aptamer-modified surface, $K_d$ is the complex dissociation constant, and [DA] is the dopamine concentration.

The Langmuir isotherms consistent with the dopamine binding to the aptamer sensing layers, prepared *via* 0.5 and 2 h aptamer immobilization, level at 2.68 ± 0.4 pmol $cm^{-2}$ (a monolayer of electrostatically adsorbed aptamer) and 1.86 ± 0.12 pmol $cm^{-2}$ (the absolute aptamer surface coverage exceeds a monolayer),[9] respectively, with the dopamine adsorption region (for 0.5 h) now being extended to 2 μM due to the improved dopamine-binding ability of the aptamer (Fig. 4). These results reflect the improved dopamine-binding ability of the aptamer monolayer in comparison with the densely packed aptamer layers/multilayers exhibiting restricted binding ability of the aptamer.

The binding affinity, $K_b$, of the RNA aptamer immobilized onto the cysteamine SAM for dopamine was 8.1 ± 0.5 $\mu M^{-1}$ for 0.5 h aptamer immobilization time (5.3 ± 0.6 $\mu M^{-1}$ for 2 h immobilization), being in agreement with a higher specific affinity of the immobilized aptamer molecules towards dopamine and/or higher stability of the dopamine–aptamer complex. Importantly, the on-surface dissociation constant of the complex ($K_d$) of 0.12 ± 0.01 μM appeared to be one order of magnitude smaller than that for the dopamine–aptamer complex in solution, estimated by equilibrium filtration to be 1.6 ± 0.17 μM.[21] The higher complex stability at the electrode surface can be correlated with the electrostatic regulation of the extent of ligand binding, in particular, with the electrostatic screening of the RNA sugar–phosphate backbone charges in the course of the RNA aptamer adsorption onto the positively charged cysteamine SAM. This allowed the minimization of non-specific electrostatic interactions between the positively charged dopamine (and, actually, other competitive catecholamine NTs) and negatively charged RNA and to improve specific binding of dopamine to the aptamer. Similar results, on several orders of magnitude improvement of the aptamer affinity for its ligand achieved by electrostatic regulation, have been recently reported for the RNA aptamer specific for the urokinase plasminogen activator (UpA), in a 1 pM electrochemical aptamer assay for this protein cancer biomarker, whose RNA-UpA complex stability in solution is characterized by the $K_d$ in the nM range.[30]

To directly correlate the dopamine binding ability with the surface coverage of the aptamer, the dopamine surface coverage ($\Gamma_{DA}$, equivalent to the number of dopamine-active aptamer molecules) was related to the absolute aptamer surface coverage (Table 1). As can be seen, the $\Gamma_{DA}/\Gamma_{RNA}$ ratio decreased with increasing immobilization time, approaching unity at the lowest surface coverage. Therefore, the affinity of the aptamer towards dopamine indeed correlates with the surface population of the aptamer molecules: it was most pronounced at 3.5 pmol $cm^{-2}$ providing the most efficient biorecognition of dopamine by almost all aptamer molecules immobilized on the electrode surface. Specific sensitivity of dopamine analysis by the 0.5 h immobilized aptamer sensing layer, 79 A per mol of the aptamer and per M of dopamine, dropped down almost two-fold for the 2 h prepared sensor, then becoming 37 A $mol^{-1}$ $M^{-1}$ (see the slopes of the dependences in Fig. 3A, inset), which is of direct analytical importance.

**Table 1** Biorecognition activity of the surface immobilized aptamer expressed as a relationship between the dopamine and absolute aptamer surface coverages ($\Gamma_{DA}$ and $\Gamma_{RNA}$)

| Aptamer immobilization time (h) | $\Gamma_{RNA}$ (pmol $cm^{-2}$) | $\Gamma_{DA}/\Gamma_{RNA}$ |
|---|---|---|
| 0.5 | 3.5 ± 0.3 | 0.78 ± 0.03 |
| 2 | 6.3 ± 0.3 | 0.27 ± 0.04 |
| 24 | 6.7 ± 0.5 | 0.039 ± 0.003 |

Thus, at immobilization times exceeding 0.5 h, the RNA aptamer molecules form either a tightly packed RNA monolayer or a multilayer, both being less active in dopamine biorecognition and binding as compared to the monolayer formed by the lying "flat" aptamer molecules not restricted in their dopamine binding ability. Despite the fact that a fraction of the aptamer molecules in the multilayer are weakly bound and can be easily removed either by the electrode storage in the blank buffer solution (Fig. 3B, inset) or during repetitive potential cycling (data not shown), it restricts the ability of other aptamer molecules to specifically recognize and bind dopamine. After removal of weakly bound species, the aptamer-modified electrodes become maximally active towards dopamine binding. In our previous work on the specific analysis of dopamine by the aptamer-modified electrode,[9] we produced the aptamer-modified electrodes with suppressed activity and current studies show the optimal conditions that allow the surface state of the aptamer molecules minimally restricted in its dopamine binding ability (Table 1, 0.5 h immobilization).

Finally, specific analysis of dopamine with the optimized aptamer-modified electrodes (0.5 h immobilization) was performed within the dopamine concentration range where aptamer-response is dictated by specific binding of dopamine to the surface-immobilized aptamer (below 2 μM, Fig. 4, curve 2). A typical chronoamperometric response of the aptamer-modified gold electrodes to dopamine is presented in Fig. 5. As can be seen in the inset, the specific current densities of dopamine oxidation, expressed as $I/\Gamma_{RNA}$, linearly increase with the increasing dopamine concentration in the range of 0.1–2 μM. The DA detection limit for the $\Gamma_{RNA}$ of 3.5 ± 0.3 pmol $cm^{-2}$ (the optimal aptamer surface coverage) was 0.1 μM, which is twice lower than 0.2 μM obtained for $\Gamma_{RNA}$ = 6.3 ± 0.3 pmol $cm^{-2}$ (the multilayer/densely-packed aptamer-modified electrodes). The specific (*i.e.* related to the absolute aptamer surface coverage) sensitivity of dopamine analysis by the aptamer monolayer electrodes was also higher than by the

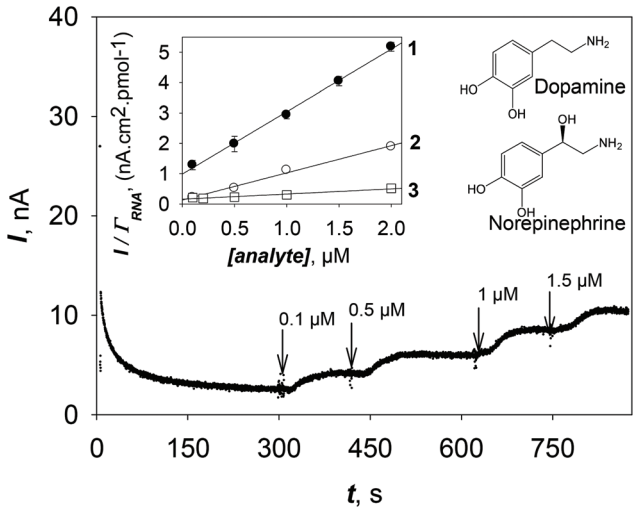


Fig. 5 Representative chronoamperogram recorded in PBS, pH 7.4, with the 0.5 h immobilized aptamer-modified electrode upon successive additions of dopamine. Inset: dependence of the specific currents of dopamine oxidation (expressed as $I/\Gamma_{RNA}$) on the dopamine concentration for (1) 0.5 and (2) 2 h aptamer-modified electrodes and (3) on the norepinephrine concentration, 0.5 h electrodes. Similar to (3) data were obtained for L-DOPA and catechol. $E_{detection}$: +0.185 V. The CA was performed in a 5 mL electrochemical cell with no stirring. The dopamine injections were done at a distance of ~3 cm from the electrode surface, so the *ca.* 20 s lag-period between the injection and response, due to the dopamine diffusion and aptamer binding, can be followed in the chronoamperogram.

densely packed aptamer electrodes, 2.05 (nA $\mu M^{-1}$)/(pmol $cm^{-2}$) *versus* 0.89 (nA $\mu M^{-1}$)/(pmol $cm^{-2}$), correlating to the general sensitivity of analysis of 85.4 and 66.8 nA $\mu M^{-1}$ $cm^{-2}$, respectively (the latter lower value is consistent with a previously reported 62 nA $\mu M^{-1}$ $cm^{-2}$).[9] Such a two-fold improvement in the detection limit and specific sensitivity of the assay significantly improves the robustness of the dopamine analysis in the presence of other NTs (Fig. 5, inset). No significant oxidation signal was detected when dopamine was replaced by the competitive NT, norepinephrine, demonstrating both the ability of the aptasensor to specifically detect dopamine and improved discrimination between dopamine and structurally related neurotransmitters with similar redox potentials (Fig. 5, inset, curve 3 *versus* curves 2 and 1). It is worth mentioning that NT discrimination ability of the aptamer-modified electrodes is much improved compared to the aptamer's ability in solution, which is insufficient for robust discrimination between, *e.g.*, dopamine and norepinephrine (based on 100% and 58% ability of these molecules to elute the dopamine–agarose-bound aptamer).[21]

The achieved sensitivity and specificity of the optimized aptamer system for dopamine analysis better satisfies the requirements for monitoring of *in vivo* fluctuations of dopamine during behavioral and pharmacological events, which generally occur in the range of 10 nM (a basal level) – 1 μM dopamine.[6] Our results evidence that dopamine binding and the resulting biosensor performance is extremely sensitive to the surface state of the aptamer molecules and their population at the electrode surface. Denser surface states of the aptamer do not obligatorily result in the best performance of the aptasensor, but *vice versa*, they result in inhibited biosensor response and lower sensitivity of the analyte due to the restricted ligand binding ability. This may be applicable to other ligand–aptamer electrode systems in which electrochemically inactive ligands unfortunately do not allow such a straightforward analysis of ligand binding by surface-tethered aptamers as demonstrated here.

Importantly, specific analysis of dopamine by the aptamer-modified electrodes currently seems to be the simplest and most reliable of the hitherto suggested approaches (Table 2) as well as most applicable for the direct analysis of dopamine levels in brain or brain tissues,[31] once the stability of the aptamer linkage to the electrode surface is increased (on conditions of either the same as demonstrated here or improved selectivity and sensitivity of analysis). SPR analysis with a dopamine receptor as a biorecognition unit[32] suggests a reasonable alternative though not for *in vivo* applications, and recently the encouraging results have been obtained with modified Si nanoparticles[33] whose fluorescence may be quenched by the oxidized dopamine molecules, through the Förster resonance energy transfer. In other sensing schemes,

Table 2 Some analytical characteristics of the existing sensors for specific analysis of dopamine in the presence of other NTs and their metabolites

| Electrode modification | LR (μM) | LOD (μM) | NT&NT metabolites | Detection method | Ref. |
|---|---|---|---|---|---|
| Au/DA-RC | 0.0006–4.6 | $5.6 \times 10^{-4}$ | DOPAC, DOPA | SPR | 32 |
| GCE/laccase//MWCNTs | 1–30 | 0.4 | DOPAC | CV, DPV | 34 |
| Au/MWCNTs//poly(AABA) | 0.05–2 | 0.02 | Tyr, HVA, DOPAC | CV, DPV, EQCM | 35 |
| HOPG | No data | No data | 5-HT | CV | 36 |
| APTMS SiNPs | 0.005–10 | $3 \times 10^{-4}$ | NE, 5-HT | Fluorescence | 33 |
| Au/Cys//RNA aptamer | 0.1–2<br>0.1–5 | 0.1 | E, NE, DOPA, DOPAC, CH, Tyr, HMP | CV, CA | This work and 9 |

AABA-3: acrylamidophenylboronic acid; APTMS SiNPs: (3-aminopropyl) trimethoxysilane silicon nanoparticles; Cys: cysteamine; CH: catechol; DA-RC-$D_3$: dopamine receptor; DOPA: 3-(3,4-dihydroxyphenyl)-alanine; DOPAC: 3,4-dihydroxyphenylacetic acid; E: epinephrine; HMP: 4-hydroxy-4-methoxyphenethylamine hydrochloride; 5-HT: serotonin; HVA: homovanillic acid; NE: norepinephrine; Tyr: tyramine; LOD: limit of detection; LR: linear range; DPV: differential pulse voltammetry; EQCM: electrochemical quartz crystal balance; SPR: surface plasmon resonance; CV: cyclic voltammetry; CA: chronoamperometry.

 

non-interfering NT species (dihydroxyphenylacetic acid, homovanillic acid, tyramine, and serotonin, see Table 2) should be either referred to NT metabolites or dopamine-unrelated NTs, whose oxidation potentials are quite different from those of dopamine and other catecholamines.[9] Thus, the possibility of specific analysis of dopamine by those assays,[34–36] in the presence of structurally related NTs, remains unclear.

## Conclusions

The surface state/surface density of the dopamine RNA aptamer immobilized at the electrodes has been shown to dramatically affect the dopamine binding ability of the aptamer, being maximal for the RNA aptamer monolayer composed of the aptamer molecules lying "flat" on the electrode surface, but not for the maximal achievable aptamer surface coverage. Electrostatic regulation of the aptamer binding to the cysteamine SAM-modified electrodes allowed the improvement of the RNA aptamer binding affinity for dopamine, with the dopamine–aptamer complex dissociation constant decreasing to 0.12 μM as compared to 1.6 μM shown in solution. 0.1–2 μM dopamine could be specifically and sensitively detected by the optimized aptamer-modified electrodes, with no interference from electrochemically/structurally related catecholamines, such as norepinephrine, L-DOPA, and catechol. The results strongly suggest that the surface state of the aptamer/its surface coverage should be considered as a critical parameter in the construction of the affinity biosensors, particularly in the case of aptamers whose biorecognition reactions can be sterically hindered by a too dense population of the aptamer molecules at the electrode surface. These results should be taken into account in the design and analysis of other aptamer–electrode systems in which an electrochemically inactive ligand does not allow direct correlation of the aptamer surface state and its binding affinity.

## Acknowledgements

This work was supported by the Danish National Research Foundation (DNRF) through their support to the CDNA, grant number DNRF8. IÁM thanks the FICYT and the 7th WP of the European Union, Marie Curie Actions, for the post-doctoral grant ACA14-22.

## Notes and references

1 J.-M. Beaulieu and R. R. Gainetdinov, *Pharmacol. Rev.*, 2011, **63**, 182–217.
2 A. Grace, *Neurosci.*, 1991, **41**, 1–24.
3 J. A. Obeso, M. C. Rodriguez-Oroz, C. G. Goetz, C. Marin, J. H. Kordower, M. Rodriguez, E. C. Hirsch, M. Farrer, A. H. Schapira and G. Halliday, *Nat. Med.*, 2010, **16**, 653–661.
4 D. Sulzer, *Neuron*, 2011, **69**, 628–649.
5 S. E. Hyman and R. C. Malenka, *Nat. Rev. Neurosci.*, 2001, **2**, 695–703.
6 A. Michael and L. Borland, in *Electrochemical Methods for Neuroscience*, ed. A. C. Michael and L. M. Borland, CRC Press, Boca Raton (FL), 2007, ch. 2.
7 J. Bicker, A. Fortuna, G. Alves and A. Falcão, *Anal. Chim. Acta*, 2013, **768**, 12–34.
8 A. Pandikumar, G. T. Soon How, T. P. See, F. S. Omar, S. Jayabal, K. Z. Kamali, N. Yusoff, A. Jamil, R. Ramaraj, S. A. John, H. N. Lim and N. M. Huang, *RSC Adv.*, 2014, **4**, 63296–63323.
9 E. Farjami, R. Campos, J. Nielsen, K. Gothelf, J. Kjems and E. E. Ferapontova, *Anal. Chem.*, 2013, **85**, 121–128.
10 N. Jia, Z. Wang, G. Yang, H. Shen and L. Zhu, *Electrochem. Commun.*, 2007, **9**, 233–238.
11 S. B. A. Barros, A. Rahim, A. A. Tanaka, L. T. Arenas, R. Landers and Y. Gushikem, *Electrochim. Acta*, 2013, **87**, 140–147.
12 R. L. McCreery, in *Volatmmetric Methods in Brain Systems*, ed. A. A. Boulton, G. B. Baker and R. N. Adams, Humana Press, Totowa, NJ, 2010.
13 K. Jackowska and P. Krysinski, *Anal. Bioanal. Chem.*, 2013, **405**, 3753–3771.
14 E. E. Ferapontova and K. V. Gothelf, *Curr. Org. Chem.*, 2011, **15**, 498–505.
15 R. White, J. Liu, M. D. Morris, F. Macazo and L. Schoukroun-Barnes, *J. Electrochem. Soc.*, 2014, **161**(5), H301–H313.
16 B. R. Baker, R. Y. Lai, M. S. Wood, E. H. Doctor, A. J. Heeger and K. W. Plaxco, *J. Am. Chem. Soc.*, 2006, **128**, 3138–3139.
17 E. E. Ferapontova, E. M. Olsen and K. V. Gothelf, *J. Am. Chem. Soc.*, 2008, **130**, 4256–4258.
18 S. V. Lemeshko, T. Powdrill, Y. Y. Belosludtsev and M. Hogan, *Nucleic Acids Res.*, 2001, **29**, 3051–3058.
19 R. Campos and E. E. Ferapontova, *Electrochim. Acta*, 2014, **126**, 151–157.
20 E. Farjami, R. Campos and E. E. Ferapontova, *Langmuir*, 2012, **28**, 16218–16226.
21 C. Mannironi, A. DiNardo, P. Fruscoloni and G. P. Tocchini-Valentini, *Biochemistry*, 1997, **36**, 9726–9734.
22 J. C. Hoogvliet, M. Dijksma, B. Kamp and W. P. van Bennekom, *Anal. Chem.*, 2000, **72**, 2016–2021.
23 G. Hartwich, D. J. Caruana, T. de Lumley-Woodyear, Y. Wu, C. N. Campbell and A. Heller, *J. Am. Chem. Soc.*, 1999, **121**, 10803–10812.
24 D. Pastré, V. Joshi, P. A. Curmi and L. Hamon, *Small*, 2013, **9**, 3630–3638.
25 A. Nabok, A. Tsargorodskaya, D. Gauthier, F. Davis, S. P. J. Higson, T. Berzina, L. Cristofolini and M. P. Fontana, *J. Phys. Chem. B*, 2009, **113**, 7897–7902.
26 A. J. Bard and L. R. Faulkner, *Electrochemical methods: fundamentals and applications*, Wiley, New York, 1980.
27 R. H. Sarma, *Nucleic Acid Geometry and Dynamics*, Pergamon Press, New York, 1980.
28 X. Zhang, M. R. Servos and J. Liu, *Langmuir*, 2012, **28**, 3896–3902.

29 G. Scatchard, *Ann. N. Y. Acad. Sci.*, 1949, **51**, 660–672.
30 M. Jarczewska, L. Kekedy-Nagy, J. S. Nielsen, R. Campos, J. Kjems, E. Malinowska and E. E. Ferapontova, *Analyst*, 2015, DOI: 10.1039/C4AN02354D.
31 D. L. Robinson, A. Hermans, A. T. Seipel and R. M. Wightman, *Chem. Rev.*, 2008, **108**, 2554–2584.
32 S. Kumbhat, D. R. Shankaran, S. J. Kim, K. V. Gobi, V. Joshi and N. Miura, *Biosens. Bioelectron.*, 2007, **23**, 421–427.
33 X. Zhang, X. Chen, S. Kai, H. Y. Wang, J. Yang, F. G. Wu and Z. Chen, *Anal. Chem.*, 2015, **87**, 3360–3365.
34 L. Xiang, Y. Lin, P. Yu, L. Su and L. Mao, *Electrochim. Acta*, 2007, **52**, 4144–4152.
35 S. Hong, L. Y. S. Lee, M. H. So and K. Y. Wong, *Electroanalysis*, 2013, **25**, 1085–1094.
36 A. N. Patel, S.-Y. Tan, T. S. Miller, J. V. Macpherson and P. R. Unwin, *Anal. Chem.*, 2013, **85**, 11755–11764.